Spectrochimica Acta Part B 124 (2016) 87–93

Contents lists available at ScienceDirect

Spectrochimica Acta Part B

journal homepage: www.elsevier.com/locate/sab

Temperature based segmentation for spectral data of laser-induced plasmas for quantitative compositional analysis of brass alloys submerged in water ☆

Tomoko Takahashi [a,*], Blair Thornton [a,b], Takumi Sato [a], Toshihiko Ohki [c], Koichi Ohki [c], Tetsuo Sakka [d]

[a] Institute of Industrial Science, The University of Tokyo, 4-6-1, Komaba, Meguro, Tokyo 153-8505, Japan
[b] Southampton Marine and Maritime Institute, University of Southampton, Burgess Road, Southampton SO16 7QF, UK
[c] OK Lab. Co. Ltd., 8-7-3, Shimorenjyaku, Mitaka, Tokyo 181-0013, Japan
[d] Department of Energy and Hydrocarbon Chemistry, Graduate School of Engineering, Kyoto University, Nishikyo-ku, Kyoto 615-8510, Japan

ARTICLE INFO

Article history:
Received 25 February 2016
Received in revised form 24 August 2016
Accepted 24 August 2016
Available online 29 August 2016

Keywords:
Laser-induced breakdown spectroscopy (LIBS)
Quantitative analysis
Principal component regression (PCR) analysis
Partial least squares (PLS) regression analysis
Liquid-phase laser ablation

ABSTRACT

This study describes a method to quantify the composition of brass alloys submerged in water using laser-induced plasmas. Principal component regression (PCR) analysis and partial least squares (PLS) regression analysis are applied to spectral measurements of plasmas generated using a long-ns duration pulse. The non-linear effects of excitation temperature fluctuations on the signals are treated as systematic errors in the analysis. The effect of these errors on the analytical performance is evaluated by applying PCR and PLS with a temperature segmented database. The results of the analysis are compared to conventional methods that do not consider the excitation temperature and it is demonstrated that the proposed database segmentation improves accuracy, with root-mean square errors of prediction (RMSEP) of 2.7% and 2.8% for Cu and Zn in the PCR model and 2.9% and 1.8% for Cu and Zn in the PLS model, respectively. The results indicate that systematic effects contribute to fluctuation of underwater plasmas, where appropriate database segmentation can improve the performance of the PCR and PLS methods.

1. Introduction

In laser-induced breakdown spectroscopy (LIBS), a high-power laser pulse is focused on a sample to create a plasma and the elemental composition of the target can be determined by analyzing the light emitted from atoms and ions of ablated material. LIBS is suitable for in-situ chemical analysis, since it does not require any sample preparation and targets can be rapidly analyzed. Due to these advantages, LIBS can be applied to in-situ analysis on land and in planetary exploration [1–4]. Whereas LIBS should be essentially applicable to elemental analysis of solids immersed in a transparent liquid, it is often reported that signal degradation is observed when targets are measured in water using a conventional laser pulse [5–7]. Enhancement of signals from solids submerged in water using a double pulse technique has been reported [8], in contrast to single pulse measurements [9,10]. However, the double pulse method is sensitive to external pressure [11,12], and it has been demonstrated that no enhancement in line emission is observed compared with measurements using a single pulse at pressures of more than 14.6 MPa for immersed solids [11] and 10 MPa for liquids [13]. Meanwhile, it has been reported that the use of a laser pulse with long duration of ≥ 100 ns can yield significant enhancements in signal quality for underwater samples [14,15]. It has further been shown that the signal enhancements for both bulk liquids [16] and submerged solids [17] are effective at pressures of up to 30 MPa. This method has been applied to in-situ real-time measurements of seawater and hydrothermal deposits at depths of more than 1000 m, using ChemiCam, a deep-sea LIBS instrument [18]. While in-situ detection of peaks of elements contained in targets in the ocean can be successfully performed using a long-pulse LIBS technique, quantification of compositions of these targets on site is still a challenging task. Since the calibration curves in atomic emission spectroscopy can be affected by the matrix [19,20], matrix matched standards are typically required. In the case of measurements of unknown samples, prior knowledge about the chemical compositions of the samples is required to prepare calibration curves, which is not practical for in-situ measurements in the field. While calibration curves have been demonstrated for specific targets under controlled conditions [21], for most general applications, the shot-to-shot fluctuations of signals

☆ Selected Paper from the 8th Euro-Mediterranean Symposium on Laser Induced Breakdown Spectroscopy (EMSLIBS 2015), Linz, Austria, 14–18 September 2015.
* Corresponding author.

http://dx.doi.org/10.1016/j.sab.2016.08.025

in underwater long-pulse LIBS can also lead to unreliable calibration curves. Since a plasma created on a target submerged in water is strongly confined, the plasma lifetime is shorter than in air [5,11], and the signals observed exhibit much larger shot-to-shot fluctuations. Calibration-free LIBS (CF-LIBS) has been introduced to determine the elemental composition without preparing calibration curves [22]. In CF-LIBS, matrix effects and signal fluctuations are theoretically corrected based on the Boltzmann distribution law and the quantification of compositions of samples in a gaseous environment has been successfully performed in a number of studies (for example, Refs. [23–25]). The compositions of major elements of brass alloys submerged in water were also determined using a CF-LIBS method with relative errors of less than 10% [26]. It should be noted that several assumptions are made in the CF-LIBS method [20]: 1) ablation is stoichiometric, 2) the plasma is optically thin, 3) local thermodynamic equilibrium of the plasma is fulfilled temporally and spatially (within a short optical window), and 4) the plasma can be modeled as a spatially homogeneous source. Additionally, peaks of all elements contained in the target need to be observed. If any of these assumptions or requirements are not satisfied, the calculation of chemical composition using CF-LIBS can be unreliable. Meanwhile, multivariate analytical techniques have been examined for quantifying compositions of targets in atomic spectroscopy [27,28]. Multivariate analysis is a statistical approach to analyze correlations between the compositions of measurement targets and their spectra. Among the techniques, principal component regression (PCR) analysis and partial least squares (PLS) regression analysis have been successfully applied to LIBS signals of rocks taken in vacuum and gaseous environments [29–32]. PCR and PLS are based on classical multivariate regression analysis, such as the classical least squares (CLS) method or the inverse least squares (ILS) method, but they extract a few latent variables from the original training dataset by finding redundancy [27]. Using these methods, statistical errors can be removed from signals in the process of reducing the dataset's dimensions. It should be noted, however, that systematic errors cannot be removed using these techniques. The fluctuations in LIBS signal intensities observed in underwater measurements can occur systematically. In fact, it was reported that variation of experimental parameters leads to fluctuation of electron temperature, electron number density, and ablation mass, which have systematic relations with signal intensity based on the Saha-Boltzmann distribution law [33]. It was also suggested in the Ref. [33] that the performance of quantification of the compositions of metal alloys from simulated spectra using artificial neural network (ANN), which is a natural computing multivariate analytical method, improved when these parameters were added to the input data for ANN. Since PCR and PLS are more sensitive to systematic errors than ANN, it is necessary to remove the significant sources of any systematic error.

In order to investigate whether multivariate analysis can be applied to underwater long-pulse LIBS measurements, the effects of systematic errors on the quantification of compositions of solids submerged in water are estimated by comparing conventional PCR and PLS, with the corresponding methods where the reference database is segmented by the excitation temperature (hereafter temperature), which is identified as a possible cause of systematic error.

2. Materials and methods

2.1. Experimental setup

The experimental setup used in this work is shown in Fig. 1. The plasma was generated on a target by a custom-built Q-Switched Nd:YAG laser with wavelength of 1064 nm, pulse energy of 5 mJ, pulse width of 150 ns, and a repetition rate of 1 Hz delivered via a 600 μm fused-silica fiber. A target is submerged in pure water 7 mm away from the face of a custom-made objective lens with 5× magnification. The diameter of the laser beam at its focal point is 120 μm. Spectroscopic measurements were performed by observing the light from the plasma along the same path used for laser delivery. The emitted light passes through a custom-built spectrograph and the spectra are recorded using an intensified charged-coupled device (ICCD, Princeton Instruments, PI-MAX 3 Gen II) from 250 nm to 570 nm at a resolution of 0.8 nm. The wavelength calibration was performed using a standard mercury lamp (Ocean Optics, HG-1). The gate width and the gate delay of the ICCD were set to 500 ns and 400 ns, respectively, where these values were found to achieve the largest signal-to-noise ratio.

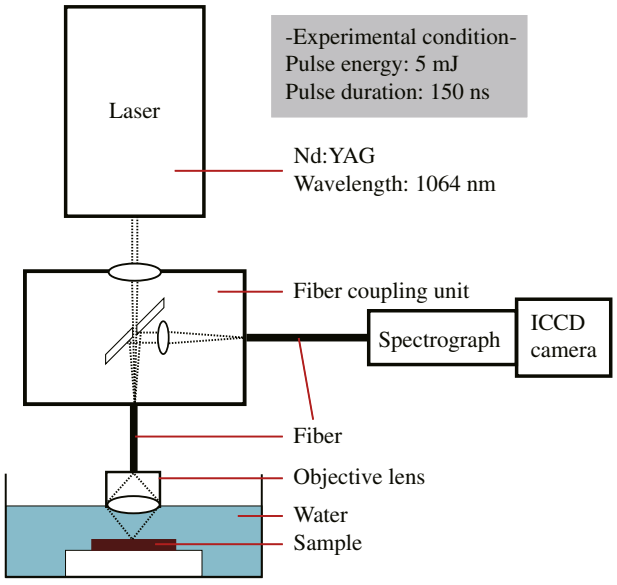

Fig. 1. Experimental setup.

2.2. Materials

A total of 11 certified brass alloys with different mass fractions of copper (Cu) and zinc (Zn) are selected for analysis (MBH Analytical Ltd., 31X7835.5, 31X7835.8, 31XB2, 31XB20, 31XB21 and 31XB23; Japan Copper and Brass Association, C5191, C2600, C6871, C2801 and C3713). The concentrations of Cu and Zn, which are major elements in the brass samples, were examined. The concentrations of Cu and Zn of the samples are shown in Table 1. These are selected to cover a broad range of concentrations (Cu; 59.6% to 93.6% and Zn; 0.02% to 39.2%) where the values for concentrations are spread relatively evenly within these ranges. The irradiation point is moved every 20 measurements in order to limit the effects of target inhomogeneity.

Table 1
Mass fractions of Cu and Zn in the certified samples.

Sample	Cu (%)	Zn (%)	Others (%)
1	91.25	6.23	2.52
2	69.93	24.83	5.24
3	60.13	39.57	0.30
4	58.53	37.03	4.44
5	69.24	29.50	1.26
6	89.57	9.97	0.46
7	93.62	0.02	6.36
8	69.89	30.10	0.01
9	78.08	21.91	0.01
10	60.48	39.50	0.02
11	59.63	39.12	1.25

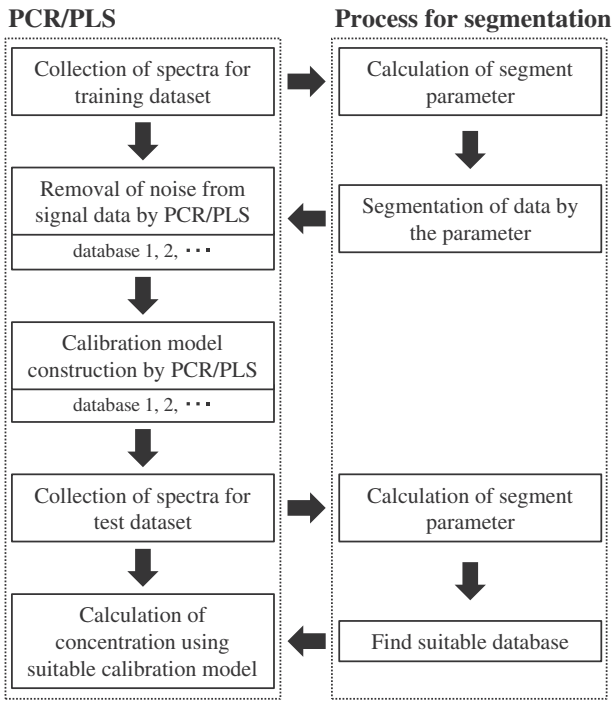

Fig. 2. Procedure of PCR and PLS calculation with segmentation of database.

2.3. Calculation of temperature and electron number density

To examine the effects of those temperature and electron number density on spectra, which are possible causes of systematic errors, temperature and electron number density are calculated for each spectrum. Temperature is calculated from each spectrum using a Boltzmann plot of three Cu I peaks, seen at 510.6 nm, 515.3 nm and 521.8 nm, which are seen in all spectra taken in this setup. The spectral line was modeled using a Lorentzian curve fit and its area was calculated by integrating the area under the Lorentzian curve after removing the continuum. The three Cu I spectral lines overlap due to broadening, and were modeled using multiple Lorentzian curves. While it is desirable to use a large number of peaks with different upper energy levels to accurately determine temperature, the Cu I lines observed at 324.8 and 327.4 nm could not be used in this study since they are susceptible to self-absorption as their lower energy levels are at the ground state. It is important to note, however, that the quantitative accuracy of the calculated temperatures does not have a direct systematic influence on the accuracy of the proposed method as would be the case in methods such as CF or CCF-LIBS. This is because temperature is used only to segment the databases used in the PCR and PLS regression analyses, where it is sufficient that the temperatures calculated are consistent between measurements. Having said that, inaccuracies in the temperatures measured are expected to introduce statistical uncertainty that limits the resolution at which the database can be reliably segmented. This in turn is expected to increase the level of uncertainty in the quantitative predictions made using the proposed technique. The electron number densities were determined from the Stark broadening effect [19] of a Zn I spectral line at 481.1 nm. The full width at half maximum of the spectral line was calculated by modeling using a Lorentzian curve fit. The method used to calculate temperature and electron number density is described in a previous publication by the authors in Ref. [26]. All calculations made in this work were implemented using MATLAB™.

2.4. Multivariate regression model

The procedure of the proposed method is shown in Fig. 2. By applying parameters for segmentation, in this case temperature or electron number density, the segmented database is constructed, where each segment contains only spectra that have those parameters within a defined range. Separate PCR and PLS models are constructed for each of the segments in the database. When the segmented model is used to characterize an unknown sample, the parameter considered in segmentation is first determined and used to select the appropriate model segment. The selected model segment is then used for quantification of compositions.

Each spectrum, which was the average of 10 spectra, was centered by subtracting the mean value of the spectrum in the regression models. The optimal numbers of principal components (PC) for the PCR model and latent variables (LV) for the PLS model are chosen to give the lowest root-mean square error of prediction (RMSEP). The samples with the highest and lowest concentrations of each element are removed when evaluating the models, so as to avoid extrapolation. For calculation of mass fractions, cross-validation of the models is performed using a standard leave-one-out cross-validation (LOOCV) procedure where 10 samples are used to train the model, and measurements of the remaining sample are used to test and verify the model.

3. Results and discussion

3.1. Data segmentation

In order to examine the effects of differences in temperature and differences in electron number density on the observed spectra, it is first necessary to decouple these terms. First, the effects of temperature were examined by choosing signals so that the average electron number density remains fixed, in this case at 2.15×10^{16} cm^{-3}, while the temperatures of the signals used remain within each temperature segment. The spectra in the database are split into 4 segments over the range from 6500 to 8500 K at an interval of 500 K for the segmented database. The spectra shown in Fig. 3 (a) are each the average of 10 signals that lie within each temperature segment, where the average electron number density of each of the averaged spectra shown remains constant. In the figure, 6750, 7250, 7750 and 8250 K indicate segments with the range from 6500 to 7000 K, from 7000 to 7500 K, from 7500 to 8000 K and from 8000 to 8500 K, respectively. Second, the effects of electron number density were examined by choosing signals so that the average temperature remains fixed, in this case at 7880 K, while the electron number densities remain within each segment of electron number density. The spectra shown in Fig. 3 (b) are each the average of 10 signals that lie within each segment of electron number density, where the average temperature of each of the averaged spectra shown remains constant. In the figure, 2.075, 2.125, 2.175 and 2.225×10^{16} cm^{-3} indicate segments with the range from 2.05 to 2.10×10^{16} cm^{-3}, from 2.10 to 2.15×10^{16} cm^{-3}, from 2.15 to 2.20×10^{16} cm^{-3}, and from 2.20 to 2.25×10^{16} cm^{-3}, respectively. In the Fig. 3 (a) and (b), spectral lines of Cu I at 324.8, 327.4, 427.5, 450.7, 453.1, 458.7, 465.1, 510.6, 515.3 and 521.8 nm, Zn I at 330.3, 334.5, 468.0, 472.2 and 481.1 nm are visible in the spectra. As seen in the figure, the peak heights and total intensities are higher for higher temperatures, while obvious differences are not seen among spectra of different electron number densities. From the results, it can be said that temperature differences have more significant effect on signals than electron number density differences.

Therefore, only temperature is considered as a parameter for data segmentation in this work. The detail results of temperature calculation of each of the samples are shown in Table 2. The results shown are the average, standard deviation, minimum temperature

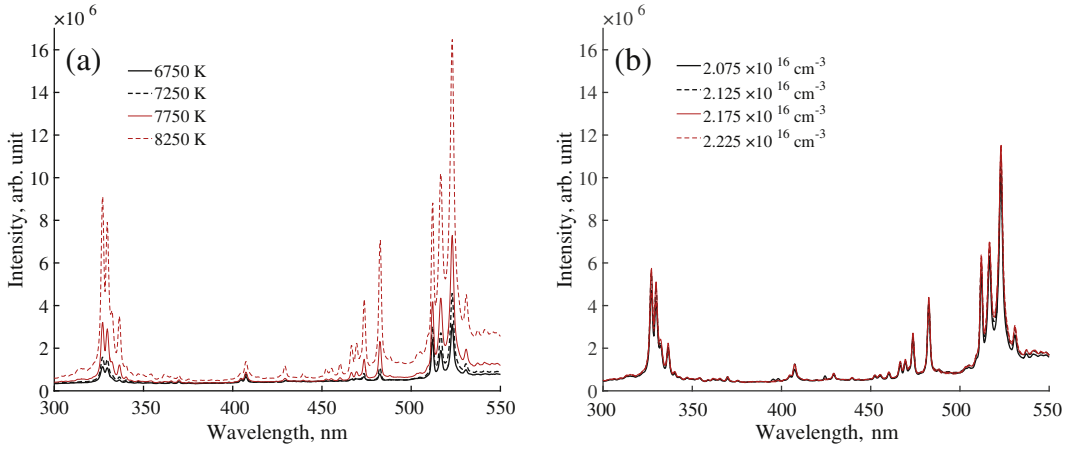

Fig. 3. Spectra of sample 2 for (a) different temperatures and (b) different electron number densities obtained in the setup. In (a), 6750, 7250, 7750 and 8250 K indicate segments with the range from 6500 to 7000 K, from 7000 to 7500 K, from 7500 to 8000 K and from 8000 to 8500 K, respectively. In (b), 2.075, 2.125, 2.175 and 2.225 × 10^{16} cm^{-3} indicate segments with the range from 2.05 to 2.10 × 10^{16} cm^{-3}, from 2.10 to 2.15 × 10^{16} cm^{-3}, from 2.15 to 2.20 × 10^{16} cm^{-3} and from 2.20 to 2.25 × 10^{16} cm^{-3}, respectively.

Table 2
Temperature calculated. Min. and max. represent minimum and maximum temperature, respectively.

Sample	Temperature (K)	Min. (K)	Max. (K)
1	7870 ± 510	6780	8730
2	7880 ± 480	6340	8660
3	7570 ± 540	6220	8700
4	8060 ± 480	6390	8720
5	7870 ± 510	6230	8810
6	7860 ± 430	6360	8660
7	8150 ± 520	6380	8930
8	7980 ± 530	6270	8880
9	8130 ± 450	6440	8940
10	7950 ± 510	6240	9000
11	7930 ± 650	6180	9140

and maximum temperature calculated from 400 spectra for each sample.

3.2. Optimal numbers of principal components/latent variables

Fig. 4 shows RMSEP as a function of the number of PC for PCR and LV for PLS. From the results of the calculation, the optimal numbers of PC which show lowest RMSEP are 5 for Cu and Zn in the conventional method, which does not account for temperature, and 6 for Cu and Zn in the proposed method, respectively, as shown in Fig. 4 (a). The optimal numbers of LV which show lowest RMSEP are 2 for Cu and 3 for Zn in the conventional method and 6 for Cu and 5 for Zn in the proposed method, respectively, as shown in Fig. 4 (b). The results are summarized in Table 3.

3.3. Calculation of mass fractions

The results of PCR analysis and PLS regression analysis are shown in Figs. 5 and 6, respectively. The results shown are the averages and standard deviations of data analyzed using the temperature segmented model, where the data for all 4 different temperatures are used. The results for data analyzed using a model constructed in the same way, but using a random dataset without temperature based segmentation, are also shown for comparison. Here the data again shows the averages and standard deviations of 4 different datasets. The grey zones in the figures represent the 95% confidence intervals.

The results show that temperature based segmentation significantly improves the analytical performance of both PCR and PLS. For PCR, the values of RMSEP for Cu and Zn are improved from 7.4% to 2.7% and from 5.7% to 2.8%, respectively. For PLS, the values of RMSEP for Cu and Zn are improved from 8.4% to 2.9% and from 6.3% to 1.8%, respectively. In addition to the RMSEP, it can also be seen that the angle of the regression line shows closer agreement with the ideal case ($y = x$) for the segmented database. The regression lines of conventional methods in all cases show small angles and large y-intercepts, which should be 1 and 0 theoretically. Here it is suggested that systematic effects underlie the results of calculation in

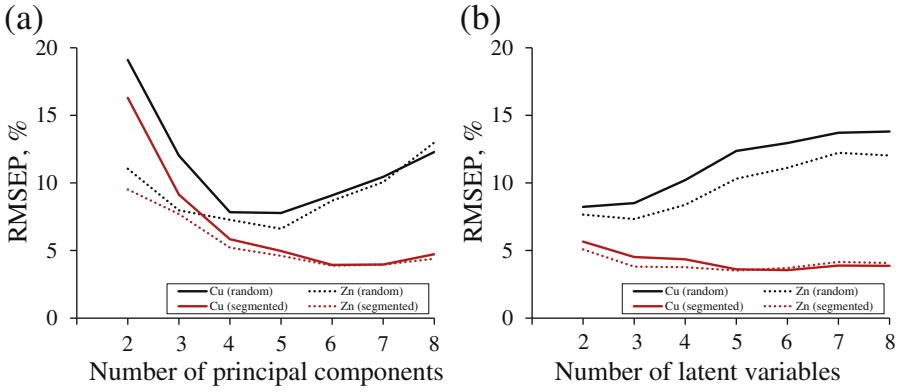

Fig. 4. Plot of the root-mean square error of prediction for the test dataset as a function of the number of (a) principal components considered in the PCR model and (b) latent variables considered in the PLS model.

Table 3
Summary of results obtained with PCR and PLS regression analysis. No. PC or LV represents optimal number of PC or LV. R^2, Slope and y-Intercept are values of regression lines.

			No. PC or LV	RMSEP (%)	R^2	Slope	y-Intercept
PCR	Random	Cu	5	7.44	0.58	0.55	31.71
	Random	Zn	5	5.66	0.82	0.72	10.02
	Segmented	Cu	6	2.66	0.95	0.92	5.18
	Segmented	Zn	6	2.81	0.95	0.98	1.67
PLS	Random	Cu	2	8.41	0.46	0.41	42.56
	Random	Zn	3	6.25	0.75	0.70	10.29
	Segmented	Cu	6	2.91	0.94	0.89	6.74
	Segmented	Zn	5	1.81	0.98	0.99	0.60

the conventional methods. Fluctuations in the data are also improved with the segmented approach having smaller error bars and significantly improved 95% confidence intervals. It should be noted, however, that a significant portion of the uncertainty is related to statistical errors rather than the systematic errors. The reason why the effects of statistical errors are also weakened in the proposed method may be due to the fact that large numbers for PC and LV are selected as optimal numbers. It is possible that when systematic errors remain in the signal datasets, larger PC and LV numbers tend to show larger RMSEP, so small numbers of PC and LV are selected as optimal numbers. However, when optimal numbers of PC and LV are not large enough to construct a regression model, not only noise but also information in the signal dataset related to construction of regression models can be discarded, which leads to unreliable calculation results. In the segmented method, since systematic errors which stem from fluctuations of temperature are removed by segmentation, more information can be extracted and modeled with large optimal numbers of PC and LV.

Comparing PCR and PLS, while differences of accuracy do not differ significantly, the accuracy of PCR is slightly higher than PLS both for Cu and Zn for the conventional methods. This might be because PLS is more sensitive to effects of systematic errors [34]. For the proposed methods, while the accuracy of Cu mass fraction calculated using PCR and PLS are almost the same, PLS is rather better than PCR in the calculation of Zn mass fraction. When systematic errors are not seen in signal datasets, mass fractions can be calculated more accurately using PLS than PCR theoretically because both signal and actual composition data are used to construct a regression model in PLS. In this case, it can be said that while systematic errors are well removed for Zn peaks by temperature based segmentation, some systematic effects remain for Cu peaks and so the accuracy of Cu mass fraction calculated using PLS are relatively similar to PCR.

4. Conclusion

This study shows that significant improvements in the analytical performance of PCR and PLS based quantification of underwater LIBS signals can be achieved by considering the temperature as a source of systematic error. The non-linear effects of temperature on the LIBS signals can be modeled by segmenting the database used to train PCR and PLS models based on temperature. The proposed method allows for rapid computation of the elemental composition of unknown samples and can potentially be used to quantify measurements on site. Presently the method has been demonstrated for Cu and Zn in brass samples that cover a wide range of concentrations. Future studies should assess the generality of the method on different sample

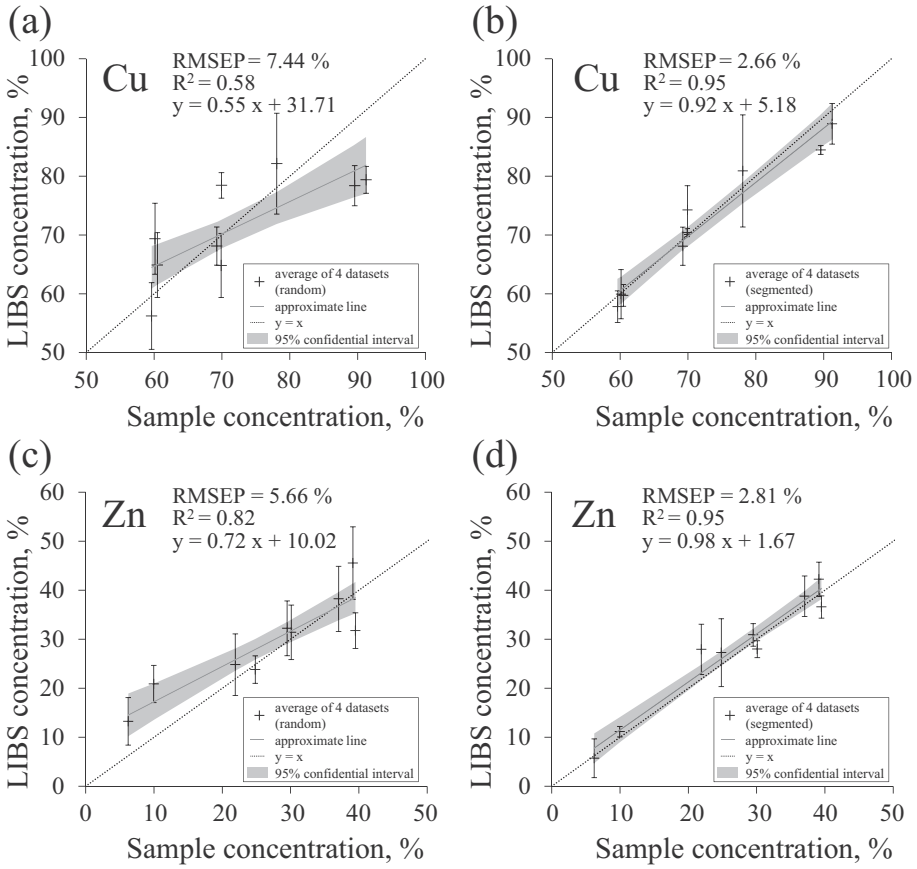

Fig. 5. PCR calibration model determined for (a) copper using the random database, (b) copper using the segmented database, (c) zinc using the random database, and (d) zinc using the segmented database.

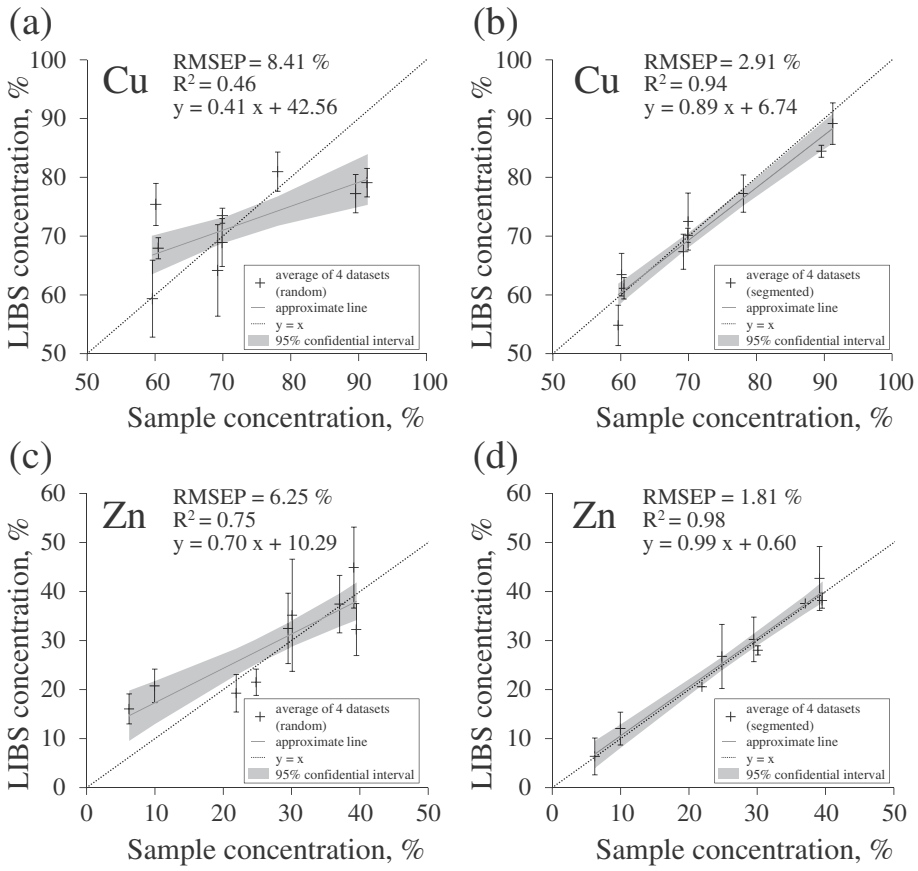

Fig. 6. PLS calibration model determined for (a) copper using the random database, (b) copper using the segmented database, (c) zinc using the random database, and (d) zinc using the segmented database.

matrices. It is also necessary to investigate the effects of database segmentation on other multivariate analytical method, such as kernel PCR and ANN to determine which of the available methods is most suitable for application to underwater measurements using long-pulse LIBS.

Acknowledgement

This project is funded by the Japanese Ministry of Education, Culture, Sports, Science and Technology under the 'Program for the development of fundamental tools for the utilization of marine resources'. Also the study was financially supported partly by JSPS Grand-in-Aid for JSPS Fellows (No.268488).

References

[1] D. Anglos, S. Couris, C. Fotakis, Laser diagnostics of painted artworks: laser-induced breakdown spectroscopy in pigment identification, Appl. Spectrosc. 51 (1997) 1025–1030.
[2] S. Rosenwasser, G. Asimellis, B. Bromley, R. Hazlett, J. Martin, T. Pearce, A. Zigler, Development of a method for automated quantitative analysis of ores using LIBS, Spectrochim. Acta B 56 (2001) 707–714.
[3] B. Sallé, J.-L. Lacour, P. Mauchien, P. Fichet, S. Maurice, G. Manhès, Comparative study of different methodologies for quantitative rock analysis by laser-induced breakdown spectroscopy in a simulated Martian atmosphere, Spectrochim. Acta B 61 (2006) 301–313.
[4] P.-Y Meslin, O. Gasnault, O. Forni, et al. Soil diversity and hydration as observed by ChemCam at Gale crater, Mars, Science (2013) 341.1238670-1-10.
[5] A.E. Pichahchy, D.A. Cremers, M.J. Ferris, Elemental analysis of metals under water using laser-induced breakdown spectroscopy, Spectrochim. Acta B 52 (1997) 25–39.
[6] A. De Giacomo, M. Dell'Aglio, F. Colao, R. Fantoni, Double pulse laser produced plasma on metallic target in seawater: basic aspects and analytical approach, Spectrochim. Acta B 59 (2004) 1431–1438.
[7] V. Lazic, F. Colao, R. Fantoni, V. Spizzicchino, Recognition of archeological materials underwater by laser induced breakdown spectroscopy, Spectrochim. Acta B 60 (2005) 1014–1024.
[8] R. Nyga, W. Neu, Double-pulse technique for optical emission spectroscopy of ablation plasmas of samples in liquids, Opt. Lett. 18 (1993) 747–749.
[9] B. Thornton, T. Ura, Effects of pressure on the optical emissions observed from solids immersed in water using a single pulse laser, Appl. Phys. Express 4 (2011)022702.
[10] B. Thornton, T. Takahashi, T. Ura, T. Sakka, Cavity formation and material ablation for single-pulse laser-ablated solids immersed in water at high pressure, Appl. Phys. Express 5 (2012)102402.
[11] A. De Giacomo, A. De Bonis, M. Dell'Aglio, O. De Pascale, R. Gaudiuso, S. Orlando, A. Santagata, G.S. Senesi, F. Taccogna, R. Teghil, Laser ablation of graphite in water in a range of pressure from 1 to 146 atm using single and double pulse techniques for the production of carbon nanostructures, J. Phys. Chem. C 115 (2011) 5123–5130.
[12] T. Takahashi, B. Thornton, T. Ura, Investigation of influence of hydrostatic pressure on double-pulse laser-induced breakdown spectroscopy for detection of Cu and Zn in submerged solids, Appl. Phys. Express 6 (2013)042403.
[13] M. Lawrence-Snyder, J. Scaffidi, S.M. Angel, A.P.M. Michel, A.D. Chave, Sequential-pulse laser-induced breakdown spectroscopy of high-pressure bulk aqueous solutions, Appl. Spectrosc. 61 (2007) 171–176.
[14] T. Sakka, H. Oguchi, S. Masai, K. Hirata, Y.H. Ogata, M. Saeki, H. Ohba, Use of a long-duration ns pulse for efficient emission of spectral lines from the laser ablation plume in water, Appl. Phys. Lett. 88 (2006)061120.
[15] T. Sakka, A. Tamura, A. Matsumoto, K. Fukami, N. Nishi, B. Thornton, Effects of pulse width on nascent laser-induced bubbles for underwater laser-induced breakdown spectroscopy, Spectrochim. Acta B 97 (2014) 94–98.
[16] B. Thornton, T. Sakka, T. Masamura, A. Tamura, T. Takahashi, A. Matsumoto, Long-duration nano-second single pulse lasers for observation of spectra from bulk liquids at high hydrostatic pressures, Spectrochim. Acta B 97 (2014) 7–12.
[17] B. Thornton, T. Sakka, T. Takahashi, A. Tamura, T. Masamura, A. Matsumoto, Spectroscopic measurements of solids immersed in water at high pressure using a long-duration nanosecond laser pulse, Appl. Phys. Express 6 (2013)082401.
[18] B. Thornton, T. Takahashi, T. Sato, T. Sakka, A. Tamura, A. Matsumoto, T. Nozaki, T. Ohki, K. Ohki, Development of a deep-sea laser-induced breakdown spectrometer for in situ multi-element chemical analysis, Deep-Sea Res. Pt. I 95 (2015) 20–36.

[19] D.W. Hahn, N. Omenetto, Laser-induced breakdown spectroscopy (LIBS), part I: review of basic diagnostics and plasma-particle interactions: still-challenging issues within the analytical plasma community, Appl. Spectrosc. 64 (2010) 335A–366A.
[20] E. Tognoni, G. Cristoforetti, S. Legnaioli, V. Palleschi, Calibration-free laser-induced breakdown spectroscopy: state of the art, Spectrochim. Acta B 65 (2010) 1–14.
[21] A. Matsumoto, A. Tamura, R. Koda, K. Fukami, Y.H. Ogata, N. Nishi, B. Thornton, T. Sakka, On-site quantitative elemental analysis of metal ions in aqueous solutions by underwater laser-induced breakdown spectroscopy combined with electrodeposition under controlled potential, Anal. Chem. 87 (2015) 1655–1661.
[22] A. Ciucci, M. Corsi, V. Palleschi, S. Rastelli, A. Salvetti, E. Tognoni, New procedure for quantitative elemental analysis by laser-induced plasma spectroscopy, Appl. Spectrosc. 53 (1999) 960–964.
[23] M. Corsi, G. Cristoforetti,V. Palleschi, A. Salvetti, E. Tognoni, A fast and accurate method for the determination of precious alloys caratage by laser induced plasma spectroscopy, Eur. Phys. J. D 13 (2001) 373–377.
[24] L. Fornarini, F. Colao, R. Fantoni, V. Lazic, V. Spizzicchino, Calibration analysis of bronze samples by nanosecond laser induced breakdown spectroscopy: a theoretical and experimental approach, Spectrochim. Acta B 60 (2005) 1186–1201.
[25] S. Pandhija, A.K. Rai, In situ multielemental monitoring in coral skeleton by CF-LIBS, Appl. Phys. B 94 (2009) 545–552.
[26] T. Takahashi, B. Thornton, K. Ohki, T. Sakka, Calibration-free analysis of immersed brass alloys using long-ns-duration pulse laser-induced breakdown spectroscopy with and without correction for nonstoichiometric ablation, Spectrochim. Acta B 111 (2015) 8–14.
[27] J. Ferré-Baldrich, R. Boqué-Martí, in: J.M. Andrade-Garda (Ed.), Basic chemometric techniques in atomic spectroscopy, Royal Society of Chemistry, Croydon, 2013, chap. 4.
[28] J.M. Andrade-Garda, A. Carlosena-Zubieta, R. Boqué-Martí, J. Ferré-Baldrich, in: J.M. Andrade-Garda (Ed.), Basic chemometric techniques in atomic spectroscopy, Royal Society of Chemistry, Croydon, 2013, chap. 5.
[29] T.F. Boucher, M.V. Ozanne, M.L. Carmosino, M. Darby Dyar, S. Mahadevan, E.A. Breves, K.H. Lepore, S.M. Clegg, A study of machine learning regression methods for major elemental analysis of rocks using laser-induced breakdown spectroscopy, Spectrochim. Acta B 107 (2015) 1–10.
[30] D.L. Death, A.P. Cunningham, L.J. Pollard, Multi-element and mineralogical analysis of mineral ores using laser induced breakdown spectroscopy and chemometric analysis, Spectrochim. Acta B 64 (2009) 1048–1058.
[31] D.L. Death, A.P. Cunningham, L.J. Pollard, Multi-element analysis of iron ore pellets by laser-induced breakdown spectroscopy and principal components regression, Spectrochim. Acta B 63 (2008) 763–769.
[32] P. Yaroshchyk, D.L. Death, S.J. Spencer, Comparison of principal components regression, partial least squares regression, multi-block partial least squares regression and serial partial least squares regression algorithms for the analysis of Fe in iron ore using LIBS, J. Anal. At. Spectrom. 27 (2012) 92–98.
[33] E.D. Andrea, S. Pagnotta, E. Grifoni, S. Legnaioli, G. Lorenzetti, V. Palleschi, B. Lazzerini, A hybrid calibration-free/artificial neural networks approach to the quantitative analysis of LIBS spectra, Appl. Phys. B 118 (2015) 353–360.
[34] T. Hasegawa, Handbook of Vibrational Spectroscopy, John Wiley & Sons Ltd. 2006, pp. 2293–2312.